

GT2013-95843

INFLUENCE OF LEADING EDGE FILLET AND NONAXISYMMETRIC CONTOURED ENDWALL ON TURBINE NGV EXIT FLOW STRUCTURE AND INTERACTIONS WITH THE RIM SEAL FLOW

Özhan H. Turgut*

Turbomachinery Aero-Heat Transfer Laboratory
Department of Aerospace Engineering
The Pennsylvania State University
University Park, Pennsylvania 16802
Email: oht101@psu.edu

Cengiz Camci†

Turbomachinery Aero-Heat Transfer Laboratory
Department of Aerospace Engineering
The Pennsylvania State University
University Park, Pennsylvania 16802
Email: cxc11@psu.edu

ABSTRACT

Three different ways are employed in the present paper to reduce the secondary flow related total pressure loss. These are nonaxisymmetric endwall contouring, leading edge (LE) fillet, and the combination of these two approaches. Experimental investigation and computational simulations are applied for the performance assessments. The experiments are carried out in the Axial Flow Turbine Research Facility (AFTRF) having a diameter of 91.66cm. The NGV exit flow structure was examined under the influence of a 29 bladed high pressure turbine rotor assembly operating at 1300 rpm. For the experimental measurement comparison, a reference Flat Insert endwall is installed in the nozzle guide vane (NGV) passage. It has a constant thickness with a cylindrical surface and is manufactured by a stereolithography (SLA) method. Four different LE fillets are designed, and they are attached to both cylindrical Flat Insert and the contoured endwall. Total pressure measurements are taken at rotor inlet plane with Kiel probe. The probe traversing is completed with one vane pitch and from 8% to 38% span. For one of the designs, area averaged loss is reduced by 15.06%. The simulation estimated this reduction as 7.11%. Computational evaluation is performed with the rotating domain and the rim seal flow between the NGV and the rotor blades. The most effective design reduced the mass averaged loss by 1.28% over the whole passage at the NGV exit.

NOMENCLATURE

- c Midspan axial chord length of nozzle guide vane.
 c_{hub} Hub axial chord length of nozzle guide vane.
 C_{P_t} Total pressure coefficient; $(P_{02} - P_{01})/(0.5 \rho V_1^2)$.
H Height of the fillet.
L Length of the fillet.
 P_0 Total pressure.
 $Re_{\theta t}$ Momentum-thickness Reynolds number.
 U_m Blade speed at mean radius.
V Velocity magnitude.
x Axial distance from nozzle guide vane leading edge.
 y^+ Non-dimensional wall coordinate; $\frac{\sqrt{\tau_w/\rho} \cdot y_p}{v}$.
 y_p First grid height off the wall.

Greek

- γ Intermittency.
 ν Kinematic viscosity.
 ρ Density.
 τ_w Wall shear stress.
 ω Turbulent frequency.

Subscripts

- 1 One axial chord upstream of nozzle guide vane leading edge.
2 Nozzle guide vane exit plane, $x/c = 1.025$.
ps Pressure side.
ss Suction side.
up Upstream

*Postdoctoral Researcher, ASME Member

†Professor of Aerospace Engineering, ASME Fellow

Abbreviations

AFTRF Axial flow turbine research facility.
LE Leading edge.
N Turbine nozzle guide vane.
NGV Nozzle guide vane.
R Turbine blade.
SST Shear stress transport.
TKE Turbulence kinetic energy.

INTRODUCTION

Sharma and Butler [1] states that the endwall losses represent 30-50% of the total pressure loss. Also, according to Denton [2], $\frac{1}{3}$ of the total aerodynamic loss in a turbine passage is governed by endwall losses. Two important parameters play a significant role in the production of endwall losses within and outside of the turbine blade: thickness of the inlet boundary layer and the amount of turning of the blade. When the incoming flow stagnates in front of a blunt object, the total pressure becomes equal to the static pressure. Hence, the flow outside the boundary layer with higher momentum tends to turn onto low momentum region closer to the endwall. As a result, a roll-up vortex occurs in front of the leading edge, and this vortex separates into two parts, known as the horseshoe vortex. The strong cross-passage pressure gradient causes the pressure side leg of horseshoe vortex to move towards the suction surface of the adjacent blade. This leg merges with the passage vortex and later on suction side leg wraps itself around this passage vortex. The strong cross-flow within the blade passage, from pressure side to suction side, feeds this flow structure, enhances it and lifts it off the endwall surface. The more detailed explanation of the secondary flows in a turbine nozzle passage can be found in [3] and [4]. It is clear from this secondary flow model that special attention should be given to the formation of the horseshoe vortex and the crossflow occurrence within the passage.

Aerodynamic losses related to this horseshoe vortex can be minimized using a leading edge fillet, which fills the intersection of the nozzle guide vane (NGV) and the hub endwall. It forms a smooth transition from the NGV leading edge to the endwall surface. These leading edge fillets are also useful from a heat transfer point of view. Minimizing the vortices results in lower mixing of the fluid near midspan and near endwall. Therefore, many researchers have been studying the effects of these leading edge fillets on turbine NGV's.

One of the earliest studies of using a leading edge modification in turbine cascades was performed by Sauer et al. [5]. The methodology was to design a bulb like geometry at the leading edge endwall junction such that the suction side leg of the horseshoe vortex became strengthened. They tested three different bulb like geometries at the intersection of the leading edge and the endwall. The results showed a 47% decrease in endwall loss. Becz et al. [6, 7] performed wind tunnel tests using Sauer

et al.'s [5] two bulb like geometries and a leading edge fillet to compare them with the baseline configuration. The large bulb geometry slightly increased the loss whereas the small bulb did not show any benefit. The leading edge fillet reduced the total pressure loss by an amount of 7.3%. Zess and Thole [8] used a fillet of one boundary layer thickness in height and two boundary layer thickness in length. They eliminated the horseshoe vortex and observed a reduction in the passage vortex. Han and Goldstein [9] designed a turbine leading edge fillet following the same design strategy of Zess and Thole [8]. The horseshoe vortex was reduced and the passage vortex was delayed. Authors also noted that the fillet increased the leading edge corner vortices on the suction and pressure sides. Shih and Lin [10] tested two different leading edge fillets claiming more than 40% reduction in the aerodynamic losses. They also reported that the surface heat transfer is reduced by 10% on the airfoil and 30% on the endwalls. The thermal benefit of leading edge fillet was also shown by Lethander et al. [11]. Although the fillet hindered the formation of the horseshoe vortex, which in turn avoided the full development of the passage vortex, the total pressure loss slightly increased. Mahmood et al. [12] experimentally investigated four different types of fillets. Based on flow visualizations, smaller horseshoe vortices occurred in front of the leading edge when compared to the baseline. Total pressure loss coefficient results, measured at a downstream location, exhibited no reduction.

This paper includes an experimental and computational investigation of the specific NGV leading edge fillets designed for the Axial Flow Turbine Research Facility (AFTRF). The aerodynamic performance of these fillets are experimentally tested on the cylindrical hub surface and also on a specific nonaxisymmetric contoured endwall designed by Turgut and Camci [13]. The experiments are performed in an HP turbine stage containing a 29 bladed rotor system rotating at 1300 rpm. The following sections will provide detailed information about the design methodology of these leading edge fillets. The aerodynamic experiments performed in this study are also supported by the computational fluid dynamics evaluation and the predictions are compared to experiments at the NGV exit.

EXPERIMENTAL FACILITY

The Axial Flow Turbine Research Facility (AFTRF) is installed at the Turbomachinery Aero-Heat Transfer Laboratory of the Pennsylvania State University. The AFTRF is a low speed, single-stage, cold flow turbine having a diameter of 91.66cm. Table 1 summarizes the design performance parameters of the turbine facility and the features are shown in Table 2. The NGV exit velocity magnitude is around $Mach = 0.3$. The detailed description and the characteristics of the AFTRF can be obtained from [14-17]. The facility is driven by four axial suction fans downstream of the rotor section and the speed of the turbine rotor is controlled by a power absorbing eddy-current brake. The

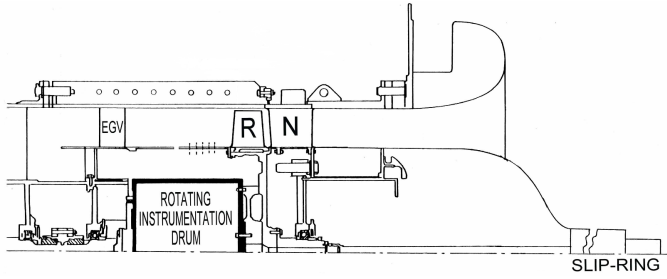


FIGURE 1: The turbine facility sketch.

TABLE 1: The AFTRF design performance parameters.

Inlet Total Temperature ($^{\circ}\text{K}$); T_{0_1}	289
Inlet Total Pressure (kPa); P_{0_1}	101.36
Mass Flow Rate (kg/s); Q	11.05
Rotational speed (rpm); N	1300
Total Pressure Ratio; P_{0_1}/P_{0_3}	1.0778
Total Temperature Ratio; T_{0_3}/T_{0_1}	0.981
Pressure Drop (mmHg); $P_{0_1} - P_{0_3}$	56.04
Hub Reaction	0.18
Pitchline Reaction	0.382
Hub Loading Coefficient; $(P_{0_1} - P_{0_3})/(1/2 \rho U_m^2)$	5.27
Pitchline Loading Coefficient	3.76
Stator Zweifel Coefficient	0.7247
Rotor Zweifel Coefficient	0.9759

inlet has a bell-mouth shape followed by the NGV row and the rotor blades. A sketch of the AFTRF is given in Fig. 1. There are 23 NGV's and 29 rotor blades followed by the exit guide vanes.

In order to test performance of the contoured endwall and the leading edge fillet designs with a reference baseline, “*Flat Insert*” is manufactured using a stereolithography (SLA) technique. This Flat Insert has a cylindrical endwall surface in the vane passage and has a thickness of 0.0075m , corresponding to $\sim 6.1\%$ of the vane span. It extends one midspan axial chord of the vane in upstream direction. It has a linear ramp upstream and with rounded edges downstream of the trailing edge to maintain surface continuity. Flat Insert ends at the rim seal with a backward facing step. The effect of backward facing step was investigated computationally in the previous paper by Turgut and Camci [18].

TABLE 2: The AFTRF design features.

Rotor Hub Tip Ratio	0.7269
Tip Radius (m); R_{tip}	0.4582
Blade Height (m); h	0.1229
Tip Relative Mach Number	0.24 (max)
Nozzle Guide Vane (tip)	
number	23
chord (m)	0.1768
spacing (m)	0.1308
turning angle	70
maximum thickness (mm)	38.81
Midspan Axial Chord	
nozzle (m)	0.1123
rotor (m)	0.09294
Vane Reynolds Number	
based on inlet velocity	$(3 \sim 4) \times 10^5$
based on exit velocity	$(9 \sim 10) \times 10^5$

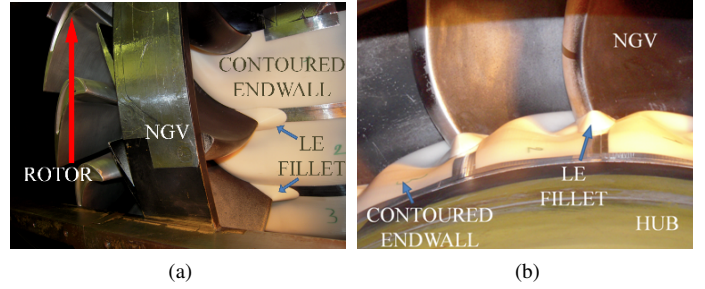


FIGURE 2: Experimental setup.

The complete stage of the AFTRF is shown in Fig. 2a. In this picture, the SLA parts of contoured endwall and one of the leading edge fillet designs are also installed in the NGV row. Figure 2b shows a view of the NGV row and the SLA parts from the upstream of the leading edge. Note that, 0.05mm (2 mils) thick aluminum tape is used for the continuity between the surfaces. SLA parts are attached to the hub surface with double-sided tape.

This paper includes the experimental investigation of the specific NGV leading edge fillets designed for the Axial Flow

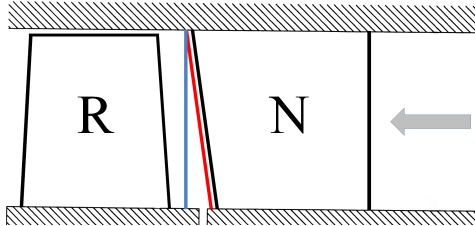


FIGURE 3: Rotor inlet plane perpendicular to axial direction and NGV exit plane parallel to NGV trailing edge.

Turbine Research Facility (AFTRF). The aerodynamic performance of these fillets are experimentally tested on the cylindrical hub surface and also on a specific nonaxisymmetric contoured endwall designed by Turgut and Camci [13]. The following sections will give detailed information about the design methodology of these leading edge fillets. The aerodynamic experiments performed in this study are also supported by the computational fluid dynamics evaluation and the predictions are presented at the NGV exit.

The blue vertical line in Fig. 3 indicates the experimental measurement plane. This axial plane is located at $x/c = 1.018$ from the NGV trailing edge at casing. The radial starting location for the measurements is selected as 8% of the vane. The reason is that the thicknesses of SLA parts downstream of the trailing edge are 6.1% of the vane span. It is also found out that above 35% of the span, the variations in measurements are minimal. Therefore, the maximum location in the radial direction is selected as 38% of the span, which helped in reducing the time needed for a complete measurement of one pitch in the circumferential direction.

The total pressure measurements are carried out by a Kiel probe manufactured by United Sensor Corporation [19]. The probe has a 3.175mm (0.125in.) head diameter. The main advantage of the Kiel probe is the extensive range of insensitivity to yaw and pitch angles. The manufacturer documents the ranges as $\pm 48^\circ$ and $\pm 45^\circ$ for yaw and pitch, respectively. Before the experiments, the probe is manually aligned with the NGV exit flow design angle, which is 70° from the axial direction. Zaccaria and Lakshminarayana [14] reported that the flow yaw and pitch angles deviate from design value within $\pm 5^\circ$. The probe is mounted on a single-axis, linear computer controlled traverser which moves in the radial direction. This linear traverser is installed on a circumferential traverser that is attached to the facility window. The slot on the window allows the circumferential traversing mechanism to complete 1.5 vane pitches. But, authors decided to traverse one full pitch in circumferential direction for time considerations. There are 18 radial and 25 circumferential locations for data collection. 450 data points are collected in total for each experiment.

The Kiel probe is connected to a variable reluctance Valinodyne pressure transducer, and the analog data from the transducer is transferred to a 12 bit data acquisition (DAQ) board. A computer program is developed using the graphical interface LabView which reads the data coming from the DAQ board and performs necessary calculations and exports the C_{Pt} values. The estimated uncertainty in C_{Pt} is $\pm 0.6\%$, for details see [20].

DESIGN METHODOLOGY

Nonaxisymmetric Endwall Contouring

Nonaxisymmetric endwall contouring is accomplished through two steps. First step is to define splines within the vane passage at various axial locations. These splines are in the form of Fourier series expansion based adjustable curves. The first three terms of the Fourier series is found to be sufficient to create highly complex and smooth circumferential curves. Secondly, these splines are imported into a solid modeling software, in which they are combined to form a three-dimensional contoured endwall surface. The detailed description of the endwall contouring design is given in a previous paper by Turgut and Camci [13]. In that paper, various contoured endwalls were presented and computationally evaluated. Among all the designs, case D14 was found to be promising. So that, it will be tested experimentally in investigation to see its influence on the total pressure distribution at the NGV exit.

Leading Edge Fillet Design

The horseshoe vortex formation and the two legs of it are not the same for all turbine blades. According to Langston [21], the separation at the saddle point depends on the blade surface pressure distribution rather than the leading edge shape. So, a particular leading edge fillet should be designed for each turbine blade depending on the pressure field. But, there are some certain design recommendations to consider while designing the fillet. Sung and Lin [22] suggested designing the fillet such that its length is greater than the height. Also, they proposed the height to be at least one boundary layer thickness for symmetric airfoils. Zess and Thole [8] tried various configurations of height to length ratio. They also examined the fillet profile and decided on using a fillet with a linear slope.

The current LE fillet designs are based on the discussions mentioned above. Figure 4 describes the LE fillet design parameters. H represents the height of the fillet in the radial direction from the cylindrical endwall based on the vane span; L_{up} , L_{ps} , and L_{ss} are the distances from leading edge, normalized by axial chord length at the hub, showing to what extent fillet is designed in upstream axial direction, along pressure and suction surfaces, respectively. In the present study, four different types of LE fillets are introduced. Two of them have a linear cross-section, and the other two have a parabolic cross-section. The linear ones are

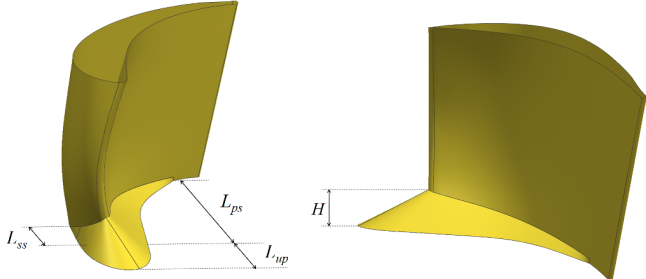


FIGURE 4: Leading edge fillet length definitions.

TABLE 3: Leading edge fillet design features.

	H / Span	L_{up} / c_{hub}	L_{ps} / c_{hub}	L_{ss} / c_{hub}
F02linear	0.08	0.27	0.28	0.22
F03curved	0.15	0.37	0.88	0.33
F03linear	0.15	0.37	0.88	0.33
F04curved	0.15	0.37	0.98	0.33
FC02linear	0.08	0.27	0.28	0.22
FC03curved	0.15	0.37	0.88	0.33
FC03linear	0.15	0.37	0.88	0.33
FC04curved	0.15	0.37	0.98	0.33

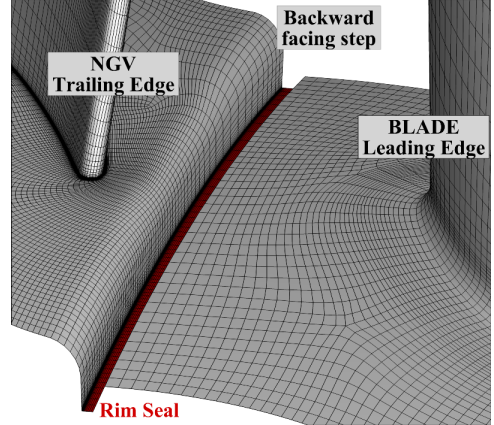


FIGURE 5: Structured grid.

COMPUTATIONAL DETAILS

The computational evaluations of the nonaxisymmetric end-walls and leading edge fillets are accomplished by the finite-volume flow solver ANSYS CFX. The steady-state, three-dimensional flow simulations are performed for the AFTRF stage including the 29 bladed rotor flow system. The numerical approach includes the stationary NGV row and the rotating blade domain. The stage interface model in CFX is used. The computational validation study of this turbine stage was performed successfully as discussed in a previous paper by Turgut and Camci [23]. The validation was established taking into account the effect of the rim seal flow between the stationary and the rotating domains. The amount of the seal flow is selected as the 0.75% of the main flow rate. Further details can be found in that paper.

The computational domain extends one midspan axial chord in the upstream direction, where the experimental inflow conditions are imposed. The circumferentially averaged total pressure and turbulence kinetic energy distribution along the span are specified at the inlet boundary according to a set of measurements from previous experimental research [17]. The mass flow rate is specified at the outflow boundary in the rotating domain. The NGV, blade and endwalls in the simulation have no-slip boundaries with adiabatic conditions.

Menter's [24] two-equation eddy-viscosity model gives good predictions especially when there is an adverse pressure gradient in the boundary layer. This shear stress transport (SST) model is based on $k-\omega$ turbulence closure formulation. Also, the flow through an uncooled NGV passage is likely to be transitional, and one should account for flow transition effects as discussed by Turgut and Camci [25]. One of the methods to predict transition is Gamma Theta model in CFX. This model is based on an empirical correlation and two more transport equations are solved; one for the momentum thickness Reynolds number ($Re_{\theta t}$), and the other for the intermittency (γ). This model is validated for various transitional flows together with SST turbulence

named as “F02linear, F03linear”, and the ones with parabolic profiles are named as “F03curved, F04curved”. These four LE fillets are designed in such a way that they are placed on a cylindrical endwall. Moreover, the performance of these fillets are also investigated on the contoured endwall, namely “FC02linear, FC03linear, FC03curved, FC04curved”. Table 3 lists the design parameters for all these designs. Figure 6 illustrates the solid model representation of LE fillets. In this figure, the Flat Insert and the LE fillets sitting on cylindrical endwall are in the left two columns; the contoured endwall and the LE fillets designed for contoured endwall are in the right two columns. F02linear and FC02linear have a design such that L_{up} is approximately twice the length of H . The remaining LE fillets have more aggressive designs which doubled the height of the fillet and extend on the pressure side and hub intersection. F03 designs elongates on the pressure side as far as $c_{hub} = 0.88$, whereas F04 designs reaches to the $c_{hub} = 0.98$ point with more filling effect on the pressure side and hub intersection corner.

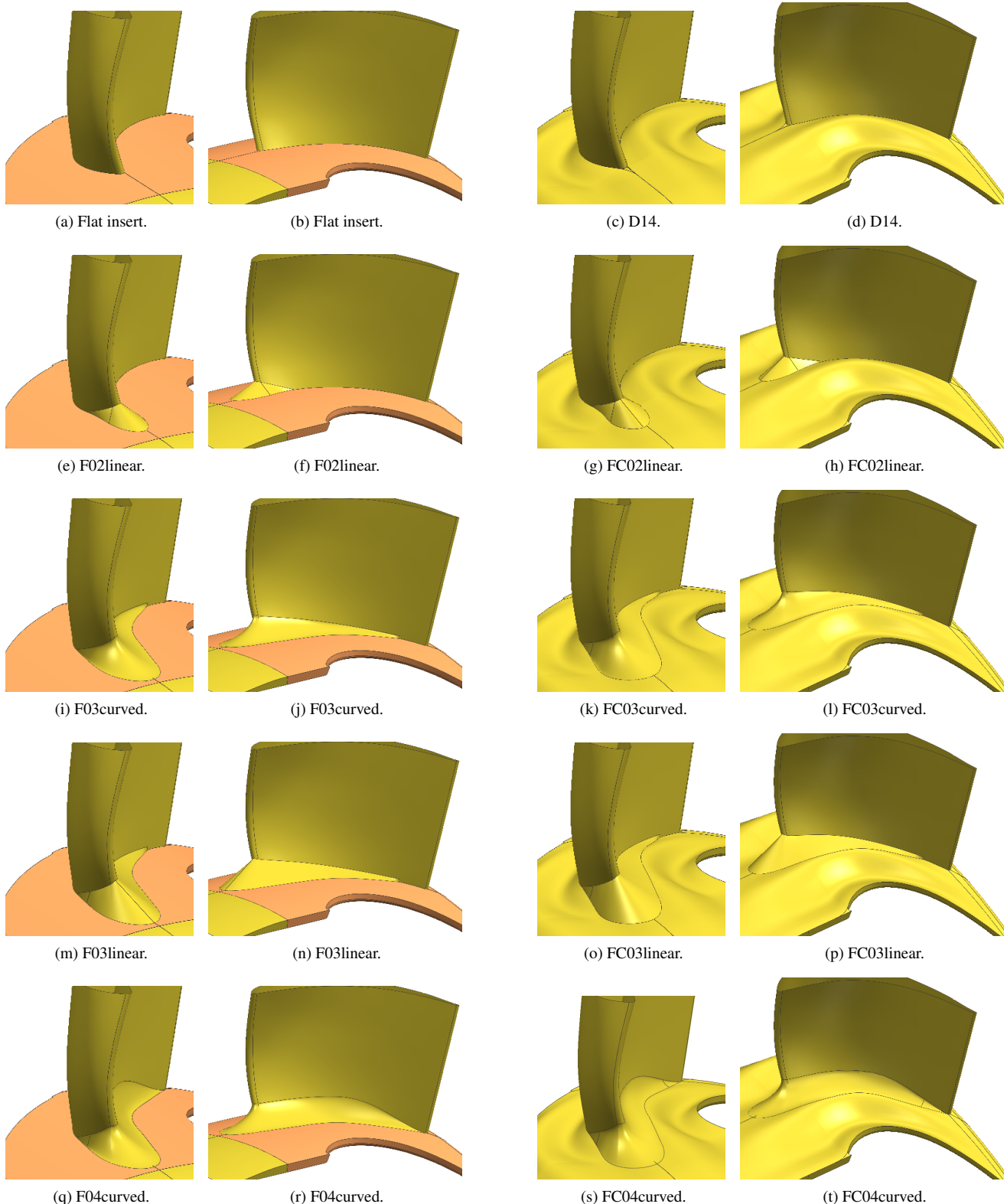


FIGURE 6: Leading edge fillet designs.

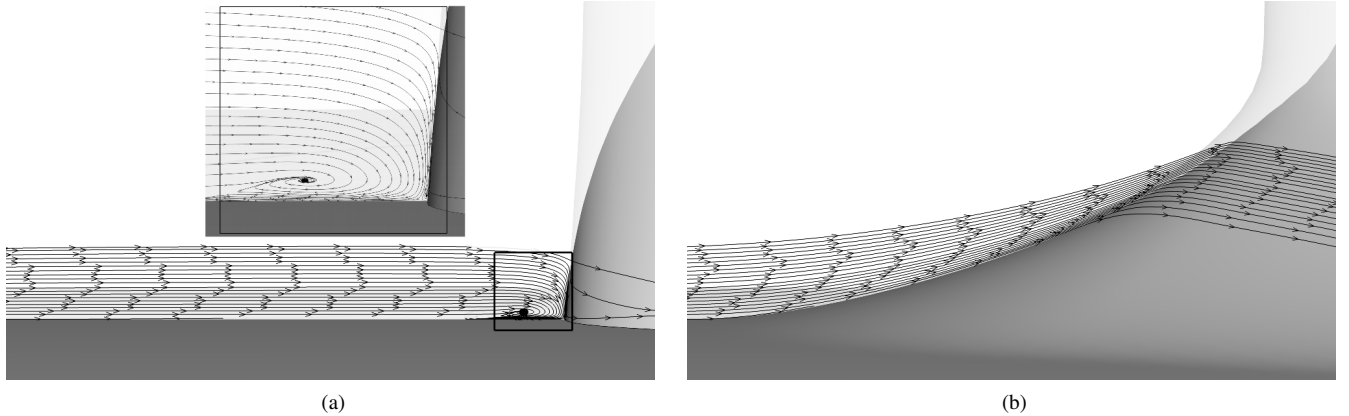


FIGURE 7: Effect of leading edge fillet on horseshoe vortex formation.

model.

Based on the discussion and previous results presented in [25], the authors applied a mesh to represent the flow field. A three-dimensional computational mesh is created by GRIDPRO. A multi-block, body-fitted structured grid gives more reasonable flow predictions in comparison to an unstructured grid, even though an unstructured mesh is easier and quicker to implement for complex turbine stage designs. Figure 5 shows a close-up view of the NGV trailing edge, the rounded backward facing step, the rim seal region, and the blade leading edge. The structured grid is well adapted to these surfaces with a sufficiently dense grid near the walls. The grid independence study was accomplished in [25]. Since the near-wall grid resolution is the key for transitional flows and for capturing the secondary flow formation, the non-dimensional wall distance of $y^+ < 1$ is satisfied everywhere in the domain. The NGV domain has 1 million and the rotor domain has 1.5 million hexahedral mesh elements.

The computational evaluation of the designs are performed on two planes. One is the rotor inlet plane where the experimental measurements were taken. The other plane is parallel to the NGV trailing edge, located at $x/c = 1.025$ away from the trailing edge line. These planes are shown in Fig. 3.

RESULTS AND DISCUSSION

Effect of Leading Edge Fillet

The purpose of using LE fillets were to minimize the horseshoe vortex formation. Figure 7 depicts how efficiently the LE fillet works. The Flat Insert endwall and LE junction is shown in Fig. 7a. A circumferential plane, extending from the leading edge in the upstream direction, is extracted and the streamlines are released on this plane. The horseshoe vortex is captured within the 5% of vane span as shown in the magnified view for a better resolution. This horseshoe vortex is completely eliminated with the use of LE fillet as shown in Fig. 7b. For both

figures, the circumferential planes and initial seed positions for the streamlines are the same. Since the flow does not meet the leading edge with a sharp corner at the hub, streamlines climb up the ramp and follow the fillet geometry nicely. Further details of the results with LE fillets will be examined at NGV exit plane and rotor inlet plane in the following sections.

Contoured Endwall, Leading Edge Fillet Designs

Four different LE fillet designs are evaluated both computationally and experimentally. These fillets are attached to the Flat Insert as well as the contoured endwall. The aim is to see the individual behavior of the fillets on a cylindrical endwall surface, and also, to analyze the performance of these designs in combination with the contoured endwall. As discussed earlier, there are two planes in which the results will be compared, namely the NGV exit plane and the rotor inlet plane.

Equal contour lines of C_{P_t} at NGV exit plane are shown in Fig. 8. There are two vertical lines and the 20% span circumferential line, which represent the edges of the secondary flow area for the Flat Insert. These lines will be used as a reference to compare the designs with the Flat Insert. The first noticeable observation is the area covered by the secondary flow is narrower for the cases D14 and the LE fillets sitting on the contoured endwall (FC series). The contoured endwall works effectively in such a way that it reduces the cross passage flow. The other apparent change is the location of the secondary flow core, which comes closer to the hub endwall in these specific cases. This is in accordance with the discussion of Turgut and Camci [18]. On the other hand, when it moves near the endwall surface, it merges with the endwall boundary layer. The loss magnitude above the hub surface increases. Also, the minimum values of C_{P_t} at the cores are 11% greater than that of the Flat Insert. The other LE fillets installed on the cylindrical endwall surface have nearly the same circumferential thickness of the secondary flow. In other words, they have the same bounding vertical lines for

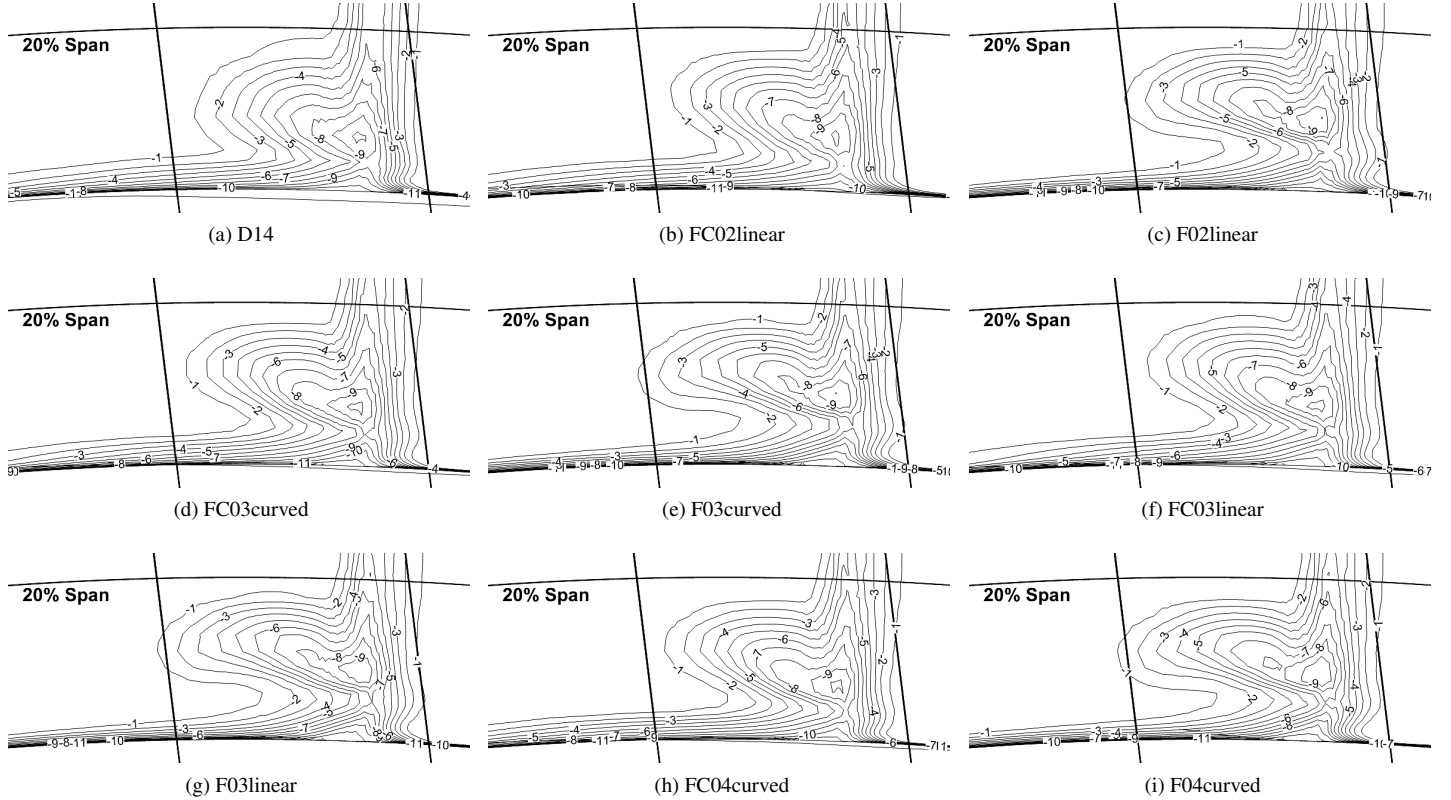


FIGURE 8: Computational C_{P_t} contours at NGV exit plane (Continued).

their secondary flow region. The upper edge of the secondary flow for these cases lie on a lower spanwise location when compared to the Flat Insert. And, from the figures it can not be said that the loss moves near the hub surface. Therefore, thickness of the secondary flow regions in the radial direction are smaller than the Flat Insert. To clarify, the secondary flow region in the Flat Insert occupies approximately 10.5% span thickness, whereas, F03curved in Fig. 8e the secondary flow has a thickness of 8% span. This explains that the LE fillets successfully minimizes the horseshoe vortex, and in turn affects the secondary flow formation. Also, filling the junction of the pressure side and the hub surface helps to reduce the crossflows, which also feed the secondary flow near the suction surface.

The circumferentially mass averaged C_{P_t} values are plotted along the span at the NGV exit and compared to the Flat Insert case as shown in Fig. 9. Note that, the distribution does not go below 6.1% span due to the existence of the Flat Insert. It is clear from these computational results that the contoured endwall has a positive influence on the distribution. D14 and the LE fillet designs installed on the contoured endwall reduce the total pressure loss above 12% span. For the D14 case, as depicted in Fig. 9a, C_{P_t} is reduced between 12-22% span, with a maximum reduction of 20%. On the other hand, it increased the loss between

8-12%. Keeping in mind that the hub surface of the Flat Insert starts at 6.1%, this increase in loss is related to the merging of the secondary flow with the hub endwall boundary layer.

F02linear slightly changed the C_{P_t} profile. There are local gains and losses in the distribution, which also affected the FC02linear performance. For instance, there is a total pressure gain between 9-12% in F02linear, and the combination of this LE fillet with the contoured endwall (FC02linear) shows an improvement in loss distribution as shown in Fig. 9b.

F03curved, F03linear, and F04curved have similar distributions as F02linear, *i.e.* loss reduction between 9-12% span, and local gains and losses above 14% span, see Figs 9c, 9d, and 9e. These LE edge fillet designs recover the extra loss generated in D14 design, near the hub endwall. Especially, FC03linear and FC03curved designs work well under 8% span to the hub surface (6.1% span). The endwall boundary layer loss is reduced in these configurations. Conversely, the local growth of loss above 14% span negatively affects the D14 performance.

The experimental measurements and the computational predictions are compared at the rotor inlet plane. The area-averaged total pressure coefficient distributions are plotted in Fig. 10. The solid lines represent the experimental data, whereas the dashed lines display computational simulation results.

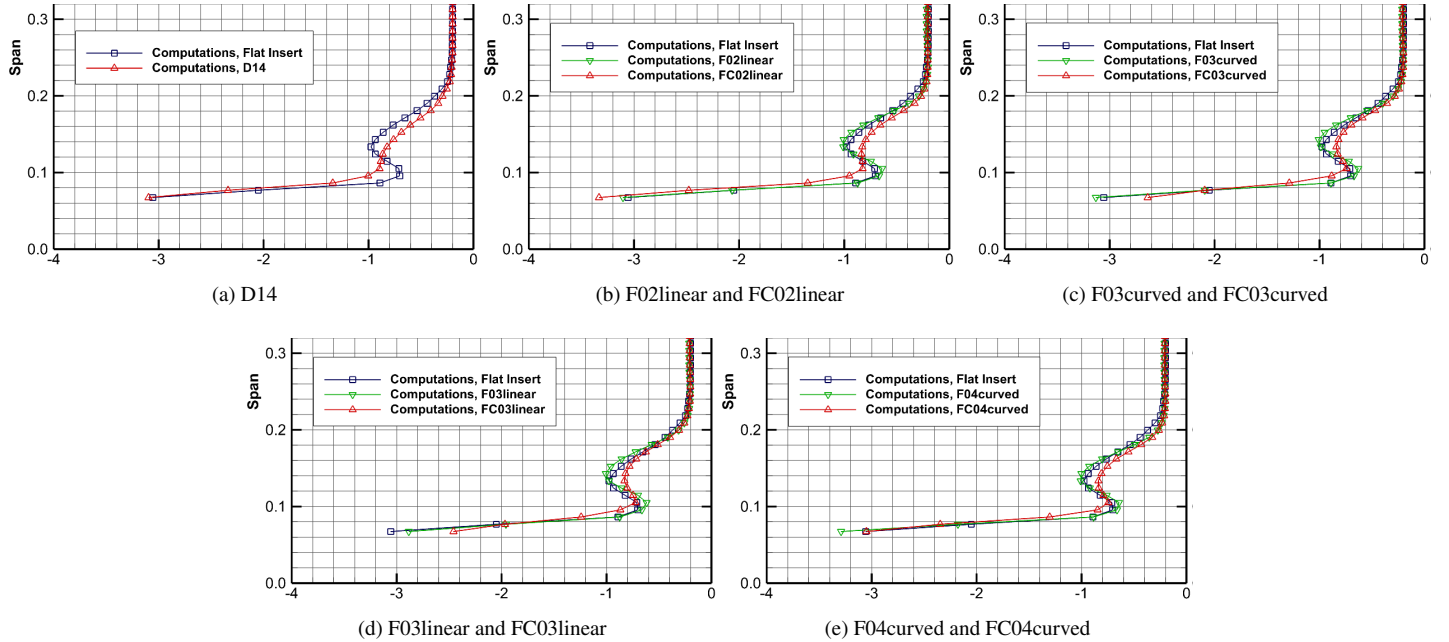


FIGURE 9: Computational C_{P_t} distributions along the span at NGV exit plane.

Figure 10a presents the C_{P_t} profile along the span for the contoured endwall D14. Experimental measurements at this rotor inlet plane resemble the NGV exit distribution as was shown in Fig. 9a. The lossy region is pulled towards the hub endwall, so the secondary flow is reduced between 15-24% span with a maximum reduction of up to 44%. But below 15% span, the total pressure coefficient is less than the Flat Insert case. The computational prediction agrees well with the measurements such that there is an improvement on loss recovery between 14-23% span with a maximum reduction of C_{P_t} approximately 23%. Again, below 13% span, the loss is increased due to more interaction with the endwall boundary layer and the rim seal flow.

FC02linear comparison shows that the experiments and the computational predictions have similar trends in the C_{P_t} spanwise profile, as shown in Fig. 10b. There is a loss recovery in the secondary flow region, an increase in C_{P_t} magnitude closer to the endwall. Maximum gain in measurements is about 40%, whereas it is 19% in numerical computations.

F02linear has the same LE fillet with FC02linear except the former sits on the cylindrical Flat Insert endwall surface. Since there is no contoured endwall in this case, the experiments showed only a little C_{P_t} improvement in the secondary flow area, as shown in Fig. 10c. The computations gave nearly the same results for F02linear and the Flat Insert.

FC03curved, like D14 and FC02linear, has a positive effect on secondary flow as shown in Fig. 10d, reaching up to 30% reduction in total pressure loss. The comparison of Figs. 10a

and 10d reveals that the most important feature of FC03curved is the recovery of the extra loss generated by the contoured endwall near the hub surface. The computational results showed an improvement between 13-23% span, but conversely it slightly increased the loss near the endwall.

F03curved works similar to FC03curved near the endwall in decreasing the C_{P_t} magnitude, as seen in Fig. 10e. Also, the secondary flow loss is reduced by a maximum value of 35%. Although the computational results did not show any improvement in the secondary flow core area, the total pressure loss near hub endwall was reduced.

Figure 10f presents the experimental results of FC03linear which are parallel to FC03curved. The computations showed little loss recovery around secondary flow region.

F03linear C_{P_t} profile is shown in Fig. 10g. Even though the computational results have little or no difference in the secondary flow when compared to the Flat Insert, apparently it is working very efficiently between 8-12% span. The measurements tell that between 9-24% the total pressure loss is decreased.

FC04curved decreased the secondary loss, which is expected in this study with the contoured endwall. But, it should be noted that below 13% span, experiments turned out to give higher C_{P_t} magnitudes. Computations predict the secondary loss reduction successfully, but showed no improvement when compared to the Flat Insert.

The experimental and computational results of F04curved agrees with each other except the secondary loss region. Al-

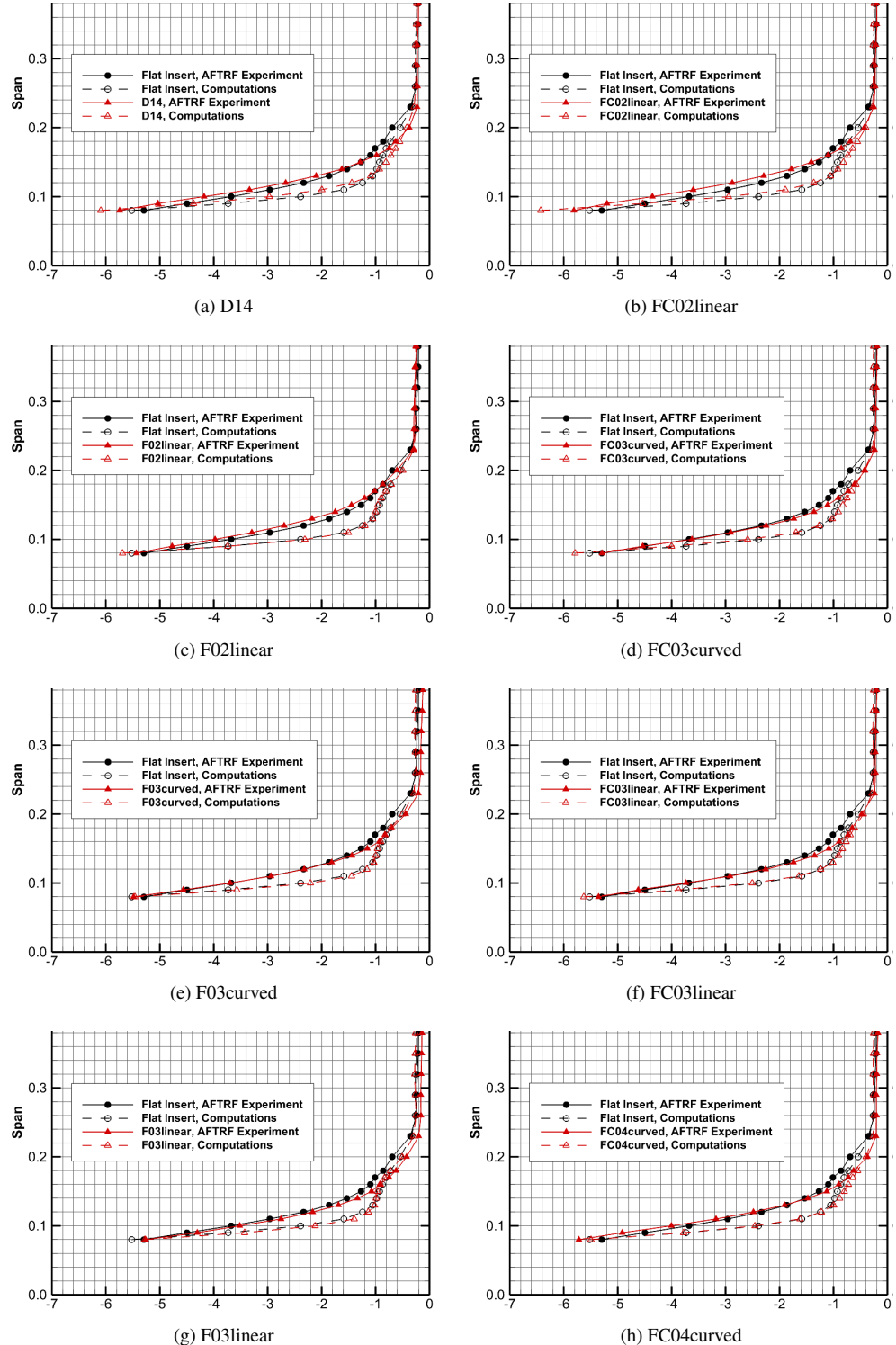


FIGURE 10: Circumferentially area-averaged C_{P_t} distribution along the span at rotor inlet plane.

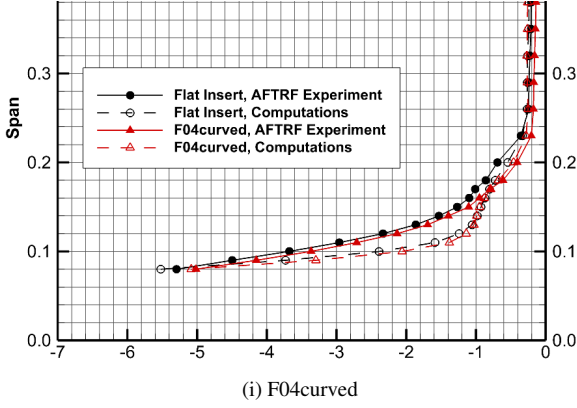


TABLE 4: Measured and computed percent changes in C_{P_t} .

	Rotor Inlet Plane		NGV Exit	
	Exp.	CFD	CFD	CFD
	Area-av.	Area-av.	Mass-av.	Mass-av.
D14	-1.08	-3.71	-2.88	1.28
FC02linear	-7.07	-4.42	-3.40	0.74
F02linear	-7.95	0.89	0.96	-0.29
FC03curved	9.18	1.60	1.79	0.93
F03curved	9.38	2.90	2.75	-0.68
FC03linear	7.43	2.42	2.48	0.90
F03linear	14.10	4.34	3.98	-0.52
FC04curved	4.28	5.41	4.43	0.57
F04curved	15.06	7.11	5.76	-0.80

FIGURE 10: Circumferentially area-averaged C_{P_t} distribution along the span at rotor inlet plane (continued).

though the measurements show an improvement, the computations do not predict it well. However, below 12% span, both claim that there is a C_{P_t} gain.

Table 4 lists the performance of the designs based on the percent change in C_{P_t} at the rotor inlet plane. These values are circumferentially averaged for one pitch from 8% to 38% vane span. Experimental measurements indicate the most efficient designs F04curved and F03linear with percent changes of 15.06 and 14.10, respectively. At the rotor inlet plane, D14, FC02linear, and F02linear do not work effectively and generate further increase in aerodynamic loss. Mass averaged results of computational effort agrees for these cases with extra loss, except for F02linear in which 0.96% improvement predicted. In simulations, the design with the most benefit is F04curved with 5.76% C_{P_t} recovery.

The NGV exit plane mass averaged C_{P_t} values are also listed in Tab. 4. The whole passage averaging shows that the endwall contouring has a favorable consequence. The contoured endwall D14 and the combination of D14 with LE fillet cases decreased the aerodynamic loss by up to 1.28%. On the other hand, LE fillets installed on cylindrical endwall increased the loss at NGV exit plane.

LE fillet designs have a tendency to weaken the crossflows from the pressure surface to the suction surface by unloading the NGV near the hub endwall. Therefore, at the NGV exit, near the hub surface the aerodynamic loss is largely recovered. This recovery was caused by the interaction of secondary flow and endwall boundary layer for the contoured endwall cases. Even though these designs do not have measurable loss reductions at the NGV exit, their positive influence can be seen at the rotor inlet plane. The Flat Insert endwall boundary layer meets with the rim seal flow after the backward facing step. The larger the momentum deficit in the upcoming boundary layer, the higher would be the mixing loss. That explains the reason that the LE

fillets give good results at the rotor inlet plane after the mixing with rim seal flow.

CONCLUSIONS

Four different LE fillets are designed for the NGV of the low-speed turbine rig, AFTRF. The performance of these new designs and the contoured endwall were tested experimentally and computationally in a turbine stage with a 29 bladed rotor disk assembly. The Flat Insert, an elevated hub surface with cylindrical surface, was used as a reference for comparison. Two sets of LE fillets were manufactured using an SLA technique. First set was installed on the Flat Insert, and the other set on the contoured endwall, D14.

The contoured endwall effectively weakened the secondary flows in the NGV passage. Mass averaged loss at the NGV exit was reduced by 1.28%. However, area averaged experimental measurement showed that it increased the loss at rotor inlet plane.

LE fillets were successful in minimizing the horseshoe vortex at the NGV LE. The fillet designs sitting on a cylindrical endwall increased the loss at the NGV exit. On the other hand, measurements showed that at the rotor inlet plane, these designs decreased the aerodynamic loss reaching up to an area averaged value of 15.06% between 8-38% vane span. The computational predictions supported this reduction by providing a mass averaged value of 5.76%.

Experimental test results of the designs involving a contoured endwall with the LE fillets showed improvements at the rotor inlet plane. One of the designs reduced the C_{P_t} value by

9.18%. For this specific design, maximum reduction of mass averaged C_{P_t} for the whole area at NGV exit was calculated to be 0.93% in the simulations.

ACKNOWLEDGMENT

The authors acknowledge the financial support provided by the Siemens Energy Inc. and thank to Dr. Matthew Montgomery, Dr. Prakash Chander, Dr. Michael Crawford, Andrew Lohaus, Anthony Malandra, Ching-Pang Lee, Boris Dobrzynski, Humberto Zuniga, Ken Landis, and Dirk Nuernberger. The authors are thankful to Dr. Ali Aktürk for his support during this study.

The content of this paper is copyrighted by Siemens Energy, Inc. and is licensed to ASME for publication and distribution only. Any inquiries regarding permission to use the content of this paper, in whole or in part, for any purpose must be addressed to Siemens Energy, Inc. directly.

REFERENCES

- [1] Sharma, O. P., and Butler, T. L., 1987. "Predictions of Endwall Losses and Secondary Flows in Axial Flow Turbine Cascades". *ASME Journal of Turbomachinery*, **109**, pp. 229–236.
- [2] Denton, J. D., 1993. "Loss Mechanisms in Turbomachines". *ASME Journal of Turbomachinery*, **115**, pp. 621–650.
- [3] Langston, L. S., Nice, M. L., and Hooper, R. M., 1977. "Three-dimensional flow within a turbine blade passage". *ASME Journal of Engineering for Power*, **99**, pp. 21–28.
- [4] Langston, L. S., 1980. "Crossflows in a turbine cascade passage". *ASME Journal of Engineering for Power*, **102**, pp. 866–874.
- [5] Sauer, H., Müller, R., and Vogeler, K., 2001. "Reduction of Secondary Flow Losses in Turbine Cascades by Leading Edge Modifications at the Endwall". *ASME Journal of Turbomachinery*, **123**, pp. 207–213.
- [6] Becz, S., Majewski, M. S., and Langston, L. S., 2003. "Leading Edge Modification Effects on Turbine Cascade Endwall Loss". *ASME Paper No. GT2003-38898*.
- [7] Becz, S., Majewski, M. S., and Langston, L. S., 2004. "An Experimental Investigation of Contoured Leading Edges for Secondary Flow Loss Reduction". *ASME Paper No. GT2004-53964*.
- [8] Zess, G. A., and Thole, K. A., 2002. "Computational Design and Experimental Evaluation of Using a Leading Edge Fillet on a Gas Turbine Vane". *ASME Journal of Turbomachinery*, **124**, pp. 167–175.
- [9] Han, S., and Goldstein, R. J., 2006. "Influence of Blade Leading Edge Geometry on Turbine Endwall Heat (Mass) Transfer". *ASME Journal of Turbomachinery*, **128**, pp. 798–813.
- [10] Shih, T. I.-P., and Lin, Y.-L., 2003. "Controlling Secondary-Flow Structure by Leading-Edge Airfoil Fillet and Inlet Swirl to Reduce Aerodynamic Loss and Surface Heat Transfer". *ASME Journal of Turbomachinery*, **125**, pp. 48–56.
- [11] Lethander, A. T., Thole, K. A., Zess, G., and Wagner, J., 2004. "Vane-Endwall Junction Optimization to Reduce Turbine Vane Passage Adiabatic Wall Temperatures". *Journal of Propulsion and Power*, **20**, pp. 1105–1116.
- [12] Mahmood, G. I., Gustafson, R., and Acharya, S., 2005. "Experimental Investigation of Flow Structure and Nusselt Number in a Low-Speed Linear Blade Passage With and Without Leading-Edge Fillets". *ASME Journal of Heat Transfer*, **127**, pp. 499–512.
- [13] Turgut, Ö. H., and Camci, C., 2011. "A Nonaxisymmetric Endwall Design Methodology for Turbine Nozzle Guide Vanes and Its Computational Fluid Dynamics Evaluation". *ASME Paper No. IMECE2011-64362*.
- [14] Zaccaria, M., and Lakshminarayana, B., 1995. "Investigation of Three-Dimensional Flowfield at the Exit of a Turbine Nozzle". *Journal of Propulsion and Power*, **11**(1), January–February, pp. 55–63.
- [15] Lakshminarayana, B., Camci, C., Halliwell, I., and Zaccaria, M., 1996. "Design and Development of a Turbine Research Facility to Study Rotor-Stator Interaction Effects". *International Journal of Turbo and Jet Engines*, **13**, pp. 155–172.
- [16] Camci, C., 2004. "Experimental and Computational Methodology for Turbine Tip De-sensitization". *VKI Lecture Series 2004-02, Turbine Blade Tip Design and Tip Clearance Treatment*.
- [17] Zaccaria, M. A., 1994. "An Experimental Investigation Into the Steady and Unsteady Flow Field in an Axial Flow Turbine". PhD Thesis, The Pennsylvania State University, University Park, PA.
- [18] Turgut, Ö. H., and Camci, C., 2012. "Experimental Investigation of Contoured Endwall and Leading Edge Fillet Configurations and Computational Evaluation". *ASME Paper No. GT2012-69304*.
- [19] United Sensor Corporation, Kiel Probes. See also URL: <http://www.unitedsensorcorp.com/kiel.html>.
- [20] Turgut, Ö. H., 2011. "Nonaxisymmetric Endwall Contouring and Leading Edge Modifications on Turbine Nozzle Guide Vanes". PhD Thesis, The Pennsylvania State University, University Park, PA, December.
- [21] Langston, L. S., 2001. "Secondary Flows in Axial Turbines-A Review". *Heat Transfer in Gas Turbine Systems, Annals of the New York Academy of Sciences*, **934**, pp. 11–26.
- [22] Sung, C.-H., and Lin, C.-W., 1998. "Numerical Investigation on the Effect of Fairing on the Vortex Flows Around Airfoil/Flat-Plate Junctures". *AIAA Paper No. AIAA-88-*

0615.

- [23] Turgut, Ö. H., and Camci, C., 2012. “Computational Validation of the Flow Through a Turbine Stage and the Effects of Rim Seal Cavity Leakage on Secondary Flows”. *ASME Paper No. GT2012-69306*.
- [24] Menter, F. R., 1994. “Two-Equation Eddy-Viscosity Turbulence Models for Engineering Applications”. *AIAA Journal*, **32**(8), pp. 1598–1605.
- [25] Turgut, Ö. H., and Camci, C., 2011. “A Computational Validation of Turbine Nozzle Guide Vane Aerodynamic Experiments in an HP Turbine Stage”. *ASME Paper No. IMECE2011-64352*.